Preparation of Cu-based Bulk Metallic Glass Matrix Composites

Yufeng SUN[1,2], *Yuren WANG*[2]†, *Bingchen WEI*[2] *and Weihuo LI*[2]

1) Research Center for Materials, Department of Materials Science and Engineering, Zhengzhou University, Zhengzhou 450002, China

2) National Microgravity Laboratory, Institute of Mechanics, Chinese Academy of Sciences, Beijing 100080, China

[Manuscript received November 8, 2004, in revised form March 21, 2005]

$Cu_{47}Ti_{34}Zr_{11}Ni_8$ bulk metallic glass (BMG) matrix composites containing *in situ* formed TiC particles and δ-TiCu dendrite phase were developed by copper mold cast. The thermal stability and microstructure of the composites are investigated. Room temperature compression tests reveal that the composite samples exhibit higher fracture strength and distinct plastic strain of 0.2%~0.5%, comparing with that of the corresponding $Cu_{47}Ti_{34}Zr_{11}Ni_8$ monolithic BMG.

KEY WORDS: Bulk metallic glasses; Shear bands; Mechanical properties; Composites

1. Introduction

Recently, bulk metallic glasses (BMGs) have drawn much attention due to their unique properties, such as high strength, perfect elastic behavior, excellent corrosion resistance and good magnetic properties. Up to now, several BMG alloy families based on La, Pd, Zr, Mg and Cu have been developed, which exhibit very good glass forming ability (GFA) and require very low cooling rate of less than 100 K/s to solidify into a glass. Some BMG alloys have already been used as sports and communication parts[1~4]. However, the lack of deformation homogeneity of BMGs at room temperature often results in inferior mechanical properties or accidental failure, which greatly limits its use as engineering structural materials[5]. It is well known that the plasticity of BMGs is dominated by the amount of shear bands. For monolithic BMG, only a single or very few shear bands could be active before failure under uniaxial quasistatic loading at room temperature. The plastic deformation of amorphous alloys is often accompanied with the pseudo-melting phenomenon on the maximum shear stress plane, which results in the appearance of vein pattern in the fractured surface[6~8]. The status of the vein patterns also can reflect the shearing direction when fracture occurs.

With the aim of improving the mechanical properties without macroscopic embrittlement, recent attempts to introduce second phase into the amorphous matrix have been carried out, which results in the development of a new kind of material, the BMG matrix composite. The second phase in the BMG composite can restrict the propagation of single shear band and facilitate the formation of multiple shear bands[9~13]. BMG matrix composites can be obtained by various methods including *in situ* formation of precipitates from the melt during casting. The *in situ* reaction during sample preparation has been considered to be effective for good wettability and homogenization of the precipitates because the *in situ* reaction can avoid the agglomeration among precipitates and form a close-banded interface between the second phase and the amorphous matrix. For example, $Zr_{56.2}Ti_{13.8}Nb_{5.0}Cu_{6.9}Ni_{5.6}Be_{12.5}$ BMG composites containing ductile phase prepared by Szuecs using an *in situ* method exhibit compressive plastic strain to 8.3%[14]. Kato has found that Zr-Al-Ni-Cu BMG composites containing *in situ* ZrC particles exhibit higher fracture strength and larger plastic strain as compared with the Zr-Al-Ni-Cu single phase BMG[15,16].

$Cu_{47}Ti_{34}Zr_{11}Ni_8$ BMG was developed by Lin and can be cast into 4 mm thick amorphous strips[17]. As Ti element has the highest reactivity with graphite to form stable TiC among the four constituents elements, the TiC can be produced as the only reactant phase during melting. This paper reported our primary results on the investigation of a novel TiC reinforced $Cu_{47}Ti_{34}Zr_{11}Ni_8$ BMG composite. It is intended to elucidate the effectiveness of the *in situ* reaction between Ti and graphite to form TiC particles that were dispersed homogeneously in $Cu_{47}Ti_{34}Zr_{11}Ni_8$ BMGs and to present the improved mechanical properties of the composites.

2. Experimental

$Cu_{47}Ti_{34}Zr_{11}Ni_8$ was used as the matrix for composites. Ingots of the matrix alloy were prepared by arc melting a mixture of the corresponding elements having the purity of at least 99.95% in a Ti gettered argon atmosphere. The ingots were broken into particles with different sizes ranging from 20 to 500 μm and mixed with extra Ti and graphite powders (particles diameter under 20 μm and 99.9% purity). The extra Ti element was added to produce TiC particles in the amorphous matrix with the nominal weight fraction of 3 wt pct. The mixture was remelted for several times in the furnace to assure the completion of the *in situ* reaction Ti+C→TiC and then suction casted into a water-cooled copper mold to fabricate the $Cu_{47}Ti_{34}Zr_{11}Ni_8$ BMG composite cylinders with various diameters (1, 2, 3 and 4 mm).

† Prof., Ph.D., to whom correspondence should be addressed, E-mail: wangyr@imech.ac.cn.

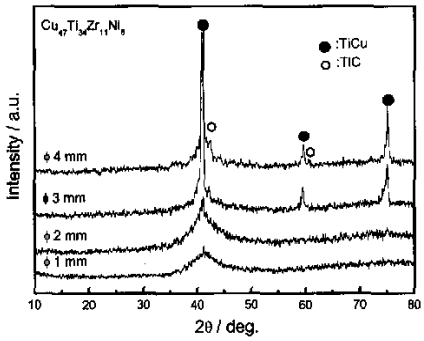

Fig.1 X-ray spectra of the as-cast $Cu_{47}Ti_{34}Zr_{11}Ni_8$ BMG composite cylinders with different diameters of 1, 2, 3 and 4 mm

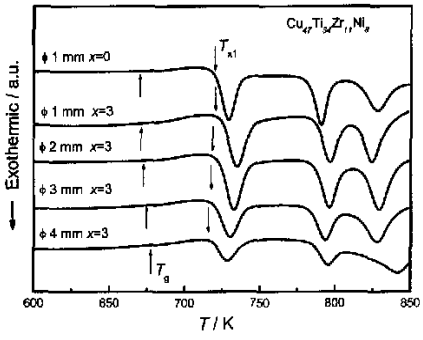

Fig.2 DSC thermogram of the as-cast $Cu_{47}Ti_{34}Zr_{11}Ni_8$ BMG composite cylinders with different diameter, (x strands for the nominal weight fraction of *in situ* TiC, wt pct)

The phase constitutions of the composites were studied by X-ray diffraction (XRD) with a Philips PW 1050 diffractometer. The thermal stability was studied using Pekin-Elmer DSC 7 calorimeter at a heating rate of 0.33 K/s. A SIRION400NC field emission scanning electron microscope (SEM) and a Jeol JSM-6400LV SEM were used for the analysis of as-cast morphologies and characterization of fracture features. SEM samples were etched using a solution of $HF:HNO_3:H_2O$=1:6:7. An OXFORD INCA300 electron microprobe analysis was used to determine the phase compositions. Room temperature compression tests on cylindrical samples with an aspect ration of 2:1 were conducted with an Instron 8562 mechanical testing device under quasistatic loading at a initial strain rate of 1×10^{-4} s^{-1}.

3. Results and Discussion

Figure 1 shows the XRD patterns of the as-cast $Cu_{47}Ti_{34}Zr_{11}Ni_8$ composite cylinders with different diameters of 1, 2, 3 and 4 mm. For the composite cylinders with the diameter of 1 mm, the XRD pattern was dominated by the typical broad amorphous peaks. Only a small crystalline diffraction peak appeared on the X-ray profile of $\phi2$ mm cylinder. For $\phi3$ mm and $\phi4$ mm cylinders, the crystalline peaks became sharper and stronger, which indicated more crystalline phase precipitated from these alloys. The crystalline phases were identified to be δ-TiCu and TiC. Furthermore, the peak intensity suggests that the amount of *in situ* TiC particles changes with the diameter of the cylinders, which reveals that more carbon elements would dissolve into the matrix with higher cooling rates.

The DSC curves of as-cast $Cu_{47}Ti_{34}Zr_{11}Ni_8$ BMG composites are shown in Fig.2, together with that of the $\phi1$ mm monolithic BMG. All samples exhibit a distinct glass transition, followed by a broad supercooled liquid region and three exothermic reactions due to crystallization. It was known that the supersaturated carbon elements and the *in situ* TiC particles could increase the viscosity of the undercooled melt[18]. This effect will give a positive contribution to the GFA of BMG. The onset of the first crystallization temperature, T_{x1}, of each sample remains unchanged with the increasing of the cylinder diameter, *i.e.*, the increasing amount of the crystalline phase. This reveals that the presence of crystalline phase does not alter the crystallization sequence of the amorphous matrix. From the DSC result, we can also see that the undercooled liquid region ΔT_x of the BMG composites becomes a little narrower with the increasing of cylinder diameter. This may results from the composition change of the amorphous matrix, which was caused by precipitation of crystalline phase. The volume fraction of the crystalline phase can be estimated by the calculation of the ratio of the heat release during annealing to the total crystallization enthalpy of the fully amorphous alloy from DSC curves. The resultant volume fractions of the crystalline phases are estimated to be 3%, 10%, 20% and 40% for $\phi1$ mm, $\phi2$ mm, $\phi3$ mm and $\phi4$ mm composite cylinders respectively, which is shown in Table 1.

The microstructures of the chemically etched cross-section for the $Cu_{47}Ti_{34}Zr_{11}Ni_8$ BMG composite cylinders are shown in Fig.3. Only blocky particles with size of 5 μm can be observed for $\phi1$ mm cylinder, which is shown in Fig.3(a). The blocky particle is proved to be TiC phase by EDS analysis. For the cylinders with diameter larger than 1 mm, TiC particles and dendrite phase could both be found, which are shown in Fig.3(b)~(d). Moreover, the size of the dendrite phase increases with increasing the diameter of the composite cylinder, namely, from 5 μm for $\phi2$ mm cylinders to 15 μm for $\phi4$ mm cylinders. The volume fraction of the dendrite phase also becomes larger with increasing the diameter of the composites cylinder, which is consistent with the result calculated from the DSC curves. EDS element analysis combined with XRD results reveal that the dendrite phase is δ-TiCu compound with a composition of 38.5Cu, 42.7Ti, 9.16Zr and 9.71Ni (in at. pct). The composition of the amorphous matrix changes slightly with the variation of the cylinder diameter. For $\phi3$ mm composite cylinder, the amorphous matrix composition is about 45.7Cu, 36.5Ti, 10.4Zr and 7.35Ni (in at. pct), which is almost the same composition of original fully amorphous alloy. The dendrite δ phase in

Table 1 Glass transition temperature (T_g), crystallization temperature (T_{x1}), supercooled temperature region (ΔT_x=T_{x1} − T_g), crystallization enthalpy (ΔH) and the volume fraction of crystalline (V_{crys}) for different cylinders

	T_g/K	T_{x1}/K	ΔT_x/K	ΔH/(J/g)	V_{crys}/%
full am.	671	719	48	389,6	–
ϕ1 mm	670	720	50	370.8	3
ϕ2 mm	673	717	44	355.9	10
ϕ3 mm	674	716	42	324.5	20
ϕ4 mm	677	715	38	251.1	40

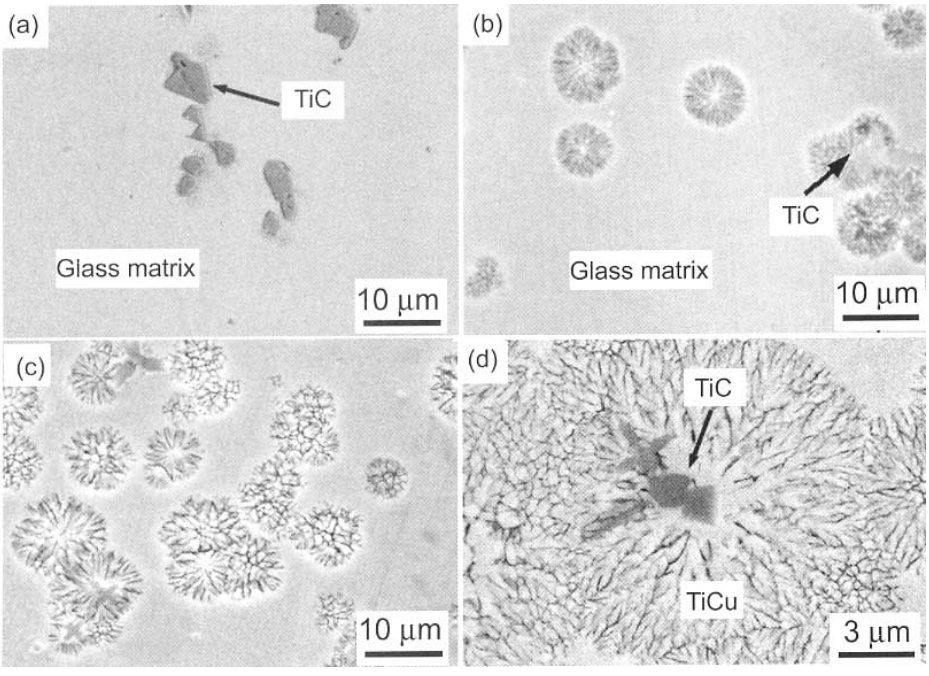

Fig.3 Microstructure of the as-cast $Cu_{47}Ti_{34}Zr_{11}Ni_8$ BMG composite cylinders with the diameter of (a) ϕ1 mm, (b) ϕ2 mm, (c) ϕ3 mm and (d) SEM backscattered image showing the TiC particles being the nucleation center of dendrite phase

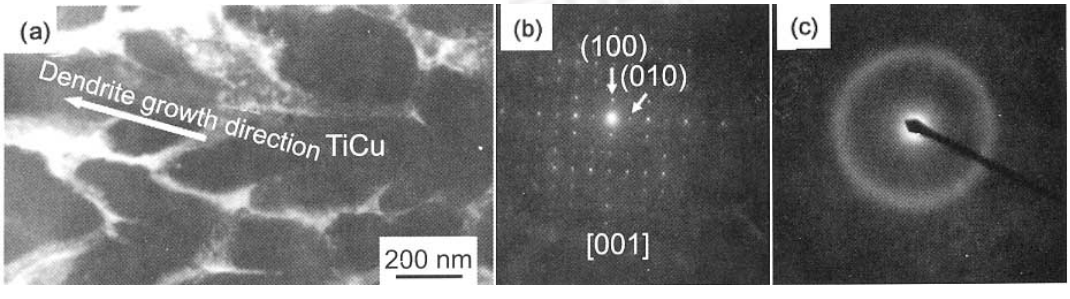

Fig.4 Bright-field TEM image of the composites showing (a) the dendrite phase, (b) SAED pattern of the dendrite phase, (c) SAED pattern of the glassy matrix

present work had round contour with vague first and second dendrite arm, and homogenously dispersed in the amorphous matrix. The formation of such a kind of structure may due to the spatially symmetric heat and mass transfer at the solid/liquid interfaces. Figure 3(d) shows the high magnification SEM backscattered image of the dendrite δ phase, with TiC particles embedded. It reveals that the TiC particles might be the nucleation center of δ phase.

From TEM image shown in Fig.4, the radius of the dendrite δ phase is determined to be about 200 nm. There is no marked change in the size of dendrites over the crosssection. The selected area electron diffraction (SAED) pattern taken along the [001] zone axis

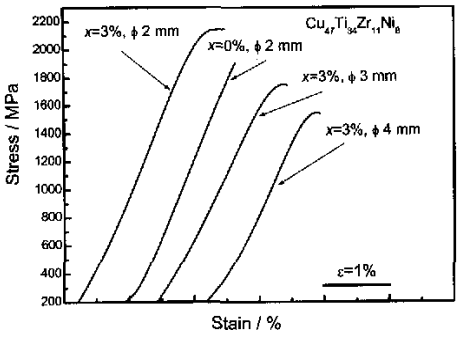

Fig.5 Room temperature compressive stress-strain curves of as-cast $Cu_{47}Ti_{34}Zr_{11}Ni_8$ BMG composites cylinders (x stand for weight fraction of TiC particles)

of the dendrite phase is shown in Fig.4(b). The white phase in Fig.4(a) is the amorphous matrix, with its SAED pattern of a broad circle shown in Fig.4(c). The presence of TiC particles on one hand certainly increase the viscosity of the undercooled melts, on the other hand may provide more heterogeneous nucleation sites. Obviously, the formation of dendrite δ phase is the result of competing nucleation among δ phase, amorphous phase and ternary or quaternary Laves phases. In this work, TiC particles will first *in situ* form during the cooling process and act as the effectively nucleation center of dendrite δ phase. So, although it is said the ternary/quaternary Laves phase shows the greatest ease of nucleation during the cooling process of $Cu_{47}Ti_{34}Zr_{11}Ni_8$ alloy melts[17], the presence of TiC particles caused the dendrite δ phase to precipitate preferentially. Therefore, the solidification process can be confirmed that the TiC particles first *in situ* formed from the alloy melt upon cooling from the high temperature melt. Then the alloy melts undergoes partial crystallization by nucleation and subsequent dendrite growth of the dendrite δ phase. The remaining liquid subsequently freezes to the amorphous state.

A series of compression tests have been carried out for the as-cast $Cu_{47}Ti_{34}Zr_{11}Ni_8$ BMG composite cylinders. Figure 5 shows typical room temperature compressive stress-strain curves of the composites cylinders, together with the data of $Cu_{47}Ti_{34}Zr_{11}Ni_8$ monolithic BMG. As seen from the S-S curve, the amorphous $Cu_{47}Ti_{34}Zr_{11}Ni_8$ alloy deforms elastically and fractures without distinct plasticity. While, the composites exhibit enhanced fracture strength σ_{max} and plastic fracture stain ε. The σ_{max} of the composite increases by 290 MPa for $\phi 2$ mm, comparing with that of the corresponding $Cu_{47}Ti_{34}Zr_{11}Ni_8$ BMG. The ε of the composites are 0.45% for $\phi 2$ mm, 0.26% for $\phi 3$ mm and 0.25% for $\phi 4$ mm cylinders, respectively.

The fracture surfaces observation of the deformed composites samples were also performed by SEM. The typical SEM images are shown in Fig.6. The vein-like pattern in the dominant shear band of the $Cu_{47}Ti_{34}Zr_{11}Ni_8$ monolithic BMG are shown in Fig.6(a), which is consistent with the observation in most metallic glasses. The vein-like structure is attributed to local softening or melting within the shear band induced by the release of high elastic energy upon instantaneous fracture. The soft or molten metallic glass within the shear bands easily flows and appears in a vein-like structure feature[19]. At room temperature, few highly developed shear bands often lead BMG to catastrophic failure and exhibit extremely low ductility under uniaxial loading. Figure 6(b) shows the SEM images of the fracture surface

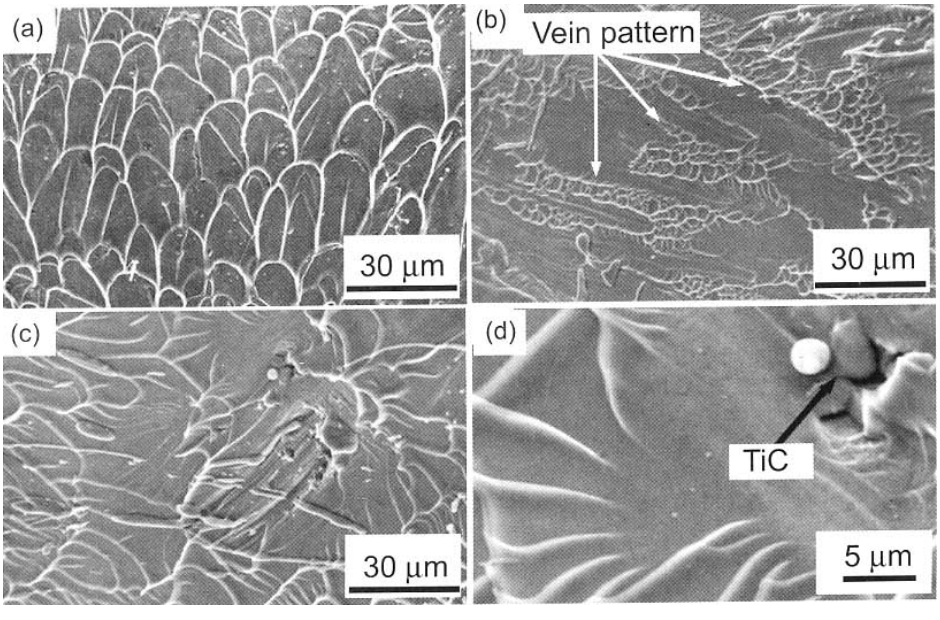

Fig.6 SEM images of the fracture surfaces (a) vein pattern of the monolithic BMG, (b) individual vein pattern in different region, (c) interaction between vein pattern and dendrite phase, (d) initiation of vein pattern around TiC particles in BMG composites

of the composite cylinders. Several individual vein patterns can be observed simultaneously in different regions, which indicted multiple shear bands might sweep through these regions. Figure 6(c) shows the interaction between the vein pattern and the dendrite phase. The development of the vein pattern was restricted and lost its typical character. The sizes of the vein patterns are different and the vein patterns extend toward different shear stress directions. The composite microstructure can also act to seed the initiation of newly organized shear band. Figure 6(d) shows the SEM image of the initiation of new shear band around TiC particles. The vein patterns generate around the particles and extend away from the particles. It was said that the plasticity of BMGs was determined by the number of shear bands. The materials will show better plasticity if more shear bands could form during the deformation process. In this paper, when the BMG matrix composite deform under compressive loading, the amorphous matrix quickly reaches its elastic limit and shear bands will generate along the maximum stress plane. The residual stresses subsequently guide the shear bands toward the reinforcements. The reinforcements interfere with the nucleation and propagation of the shear bands in the amorphous matrix by acting as pinning centers or by inducing branching of shear bands[20]. Therefore, the propagation of the highly localized shear bands is resisted to limited regions and plasticity is distributed homogeneously among the matrix. The mechanical instability of the composites is so retarded and improved ductility has been obtained.

4. Conclusions

(1) The presence of TiC particles doesn't degrade the glass forming ability and thermal stability of the $Cu_{47}Ti_{34}Zr_{11}Ni_8$ BMG matrix. The TiC particles are blocky and act as the nucleation center of dendrite δ phase. The sizes of the dendrite δ phase increase with increasing the diameter of the composite cylinders.

(2) For all composite samples, the ultimate compression stress and the plasticity exceed that of the full $Cu_{47}Ti_{34}Zr_{11}Ni_8$ glassy alloys. The increase of ultimate compression stress is due to the composites microstructure consisting of micro-sized TiC particles and dendrite δ phase homogeneously dispersed in the glassy matrix. The increase of the global plasticity can be explained by the formation of multiple shear bands, which improves the resistance against catastrophic crack propagation.

Acknowledgements

The authors acknowledge the financial support provided by the Knowledge Innovation Program of Chinese Academy of Sciences, No.KJCX2-SW-L05 and the National Natural Science Foundation of China, No. 50101012.

REFERENCES

[1] A.Inoue: *Mater. Sci. Eng.*, 1997, **A226-228,** 357.
[2] A.Inoue: *Mater. Sci. Eng.*, 2001, **A304-306,** 1.
[3] J.F.Loffler: *Intermetallics*, 2003, **11,** 529.
[4] Z.P.Lu, H.Xu and Y.Li: *Mater. Sci. Eng.*, 2001, **A304-306,** 679.
[5] W.H.Jing and M.Atzmon: *Acta Mater.*, 2003, **51,** 4095.
[6] C.A.Pampillo and H.S.Chen: *Mater. Sci. Eng.*, 1974, **31,** 181.
[7] H.S.Chen and T.T.Wang: *J. Appl. Phys.*, 1970, **44,** 5338.
[8] Y.Yokoyama, K.Yamano and Fukanra: *Scripta Mater.*, 2001, **44,** 1529.
[9] H.Choi-yim, R.Busch and U.Koster: *Acta Mater., 1999,* **47,** 2455.
[10] H.Choi-yim, R.D.Conner and F.Szuecs: *Acta Mater.*, 2002, **50,** 2737.
[11] R.D.Conner and W.L.Johnson: *Acta Mater.*, 1998, **46,** 6089.
[12] H.Xu, C.Ngs and Y.P.Feng: *Acta Mater.*, 2003, **51,** 561.
[13] Z.Bian, G.He and G.L.Chen: *Scripta Mater.*, 2002, **46,** 407.
[14] K.Szuecs, C.P.Kim and W.L.Johnson: *Acta mater.*, 2001, **49,** 1507.
[15] H.Kato, T.Hirano and Mastsuo: *Scripta Mater.*, 2000, **43,** 503.
[16] H.Kato and A.Inoue: *Mater. Trans. JIM.*, 1997, **38,** 793.
[17] X.H.Lin and W.L.Johnson: *J. Appl. Phys.*, 1995, **78,** 6514.
[18] W.H.Wang and H.Y.Bai: *J. Appl. Phys.*, 1998, **84,** 5961.
[19] G.He, Z.F.Zhang and W.Loser: *Acta Mater.*, 2003, **51,** 2383.
[20] M.Calin, J.Eckert and L.Schultz: *Scripta Mater.*, 2003, **48,** 653.